# **RESEARCH PAPER**

# Improvement the Dispersion of TiO<sub>2</sub>-PEG Nanoparticles as Novel and Efficient UV Filter in Sunscreen Formulation

Shakhlo Yuldashova <sup>1\*</sup>, Lola Sultonova <sup>1</sup>, Zarnigor Nurova <sup>1</sup>, Zuxra Amangeldieva <sup>2</sup>, Javlon Bekpulatov <sup>3</sup>, Dilnoza Saidjalilova <sup>4</sup>, Rahmatulla Gaipnazarov <sup>5</sup>, Mavluda Achilova <sup>6</sup>, Surayyo Khasanova <sup>7</sup>, Khurshid Khakimov <sup>8</sup>, Guzal Klebleeva <sup>9</sup>, Nurbek Yaxshimuratov <sup>10</sup>, Ikramjon Masharipov <sup>11</sup>

- <sup>1</sup> Bukhara State Medical Institute, Bukhara, Republic of Uzbekistan
- <sup>2</sup> Karakalpak State University named after Berdakh, Nukus, Karakalpakstan, Republic of Uzbekistan
- <sup>3</sup> Tashkent State Technical University, Tashkent, Republic of Uzbekistan
- <sup>4</sup> Tashkent state Medical University, Tashkent, Republic of Uzbekistan
- <sup>5</sup> International Islamic Academy of Uzbekistan, Tashkent, Republic of Uzbekistan
- <sup>6</sup> Chirchik State Pedagogical University, Chirchik, Republic of Uzbekistan
- <sup>7</sup> Mamun University, Khiva, Republic of Uzbekistan
- <sup>8</sup> Bukhara State Pedagogical Institute, Bukhara, Republic of Uzbekistan
- <sup>9</sup> Samarkand State Medical University, Samarkand, Republic of Uzbekistan
- <sup>10</sup> Urgench state university, Urganch, Republic of Uzbekistan
- <sup>11</sup> Tashkent state University of Economics, Tashkent, Uzbekistan

#### ARTICLE INFO

# Article History:

Received 07 June 2025 Accepted 21 September 2025 Published 01 October 2025

# Keywords:

Dispersion Nanoparticles Sunscreen formulation TiO<sub>2</sub> UV filter

#### **ABSTRACT**

A solvent-free, microwave-assisted protocol was developed to covalently graft poly(ethylene glycol) methyl ether (Mn ≈ 2 kDa) onto anatase nanocrystals at a surface density of 1.8 chains nm<sup>-2</sup>. The resulting TiO<sub>2</sub>-PEG hybrid disperses in caprylic/capric triglyceride as  $12 \pm 3$  nm primary particles (PDI < 0.12) and retains 96 % of its grafted layer after 24 h at 40 °C, whereas emulsifier-free controls lose 29 % of PEG and flocculate to 680 nm. Solid-state <sup>13</sup>C NMR confirms Ti-O-C ether linkages, while FT-IR shows complete loss of terminal vinyl resonances, evidencing chemisorption rather than physisorption. Photocatalytic ROS generation falls to 12 % relative to P25 (below the 15% EU photo-safe threshold) and an additional 33 % suppression is observed when polyglyceryl-6-stearate is present, attributable to a co-adsorbed lamellar barrier. In-vitro SPF testing (ISO 24444:2019) reveals SPF 50 and  $\lambda = 374$  nm at only 5 wt % solids, outperforming un-coated P25 by 1.8-fold while maintaining four-star UVA coverage. Reducing the particle load to 3 wt % still yields SPF 32, validating a 40 % mineral-burden decrease without efficacy loss. The platform offers a transparent, broad-spectrum and reef-compatible UV filter that satisfies forthcoming EU low-nano mandates.

#### How to cite this article

Yuldashova S., Sultonova L., Nurova Z., Amangeldieva Z. et al. Improvement the Dispersion of TiO<sub>2</sub>-PEG Nanoparticles as Novel and Efficient UV Filter in Sunscreen Formulation. J Nanostruct, 2025; 15(4):2342-2352. DOI: 10.22052/JNS.2025.04.072

<sup>\*</sup> Corresponding Author Email: yuldashova.shaxlo@bsmi.uz

#### INTRODUCTION

Ultraviolet (UV) filters constitute the molecular backbone of modern photoprotection, intercepting high-energy photons before they can trigger the cascade of DNA lesions, protein cross-links, and reactive oxygen species that culminate in photoageing and photo-carcinogenesis [1-4]. Over the past four decades the field has migrated from the first-generation soluble organic screens now under regulatory scrutiny for endocrine-disrupting activity and coral bleaching to mineral oxides that confer broad-spectrum attenuation through a synergistic combination of absorption and Mie scattering [5-8]. Yet the very same TiO2 and ZnO that offer superb UVA/UVB blocking efficiency can agglomerate within the lipophilic continuous phase of a cosmetic emulsion, producing micronscale clusters that (i) scatter visible light and generate the undesirable "white cast", (ii) erode the declared SPF through a reduction in active

surface area, and (iii) generate photocatalytic ROS at the particle-skin interface [9-12]. These limitations have propelled a multi-disciplinary effort that now spans colloid and polymer chemistry, photo-biophysics, and dermatological nanomedicine [13]. Surface passivation with inert silica or alumina shells, doping with manganese or nitrogen to truncate charge-carrier recombination, and steric stabilization with amphiphilic block copolymers have all been explored, but each strategy introduces additional processing steps, regulatory hurdles, or compromises in sensorial elegance. polyalcohols grafting is emerging as a minimalist yet powerful alternative: the hydrophilic corona simultaneously screens surface Ti<sup>3+</sup> trap states (quenching ROS quantum yields by >80 %) and imparts steric hindrance that maintains sub-100 nm dispersions even at 30 wt% solids in capric/caprylic triglycerides. Beyond sunscreens, such TiO<sub>2</sub> and ZnO nanocomposites

# **Sunscreen Material Types**

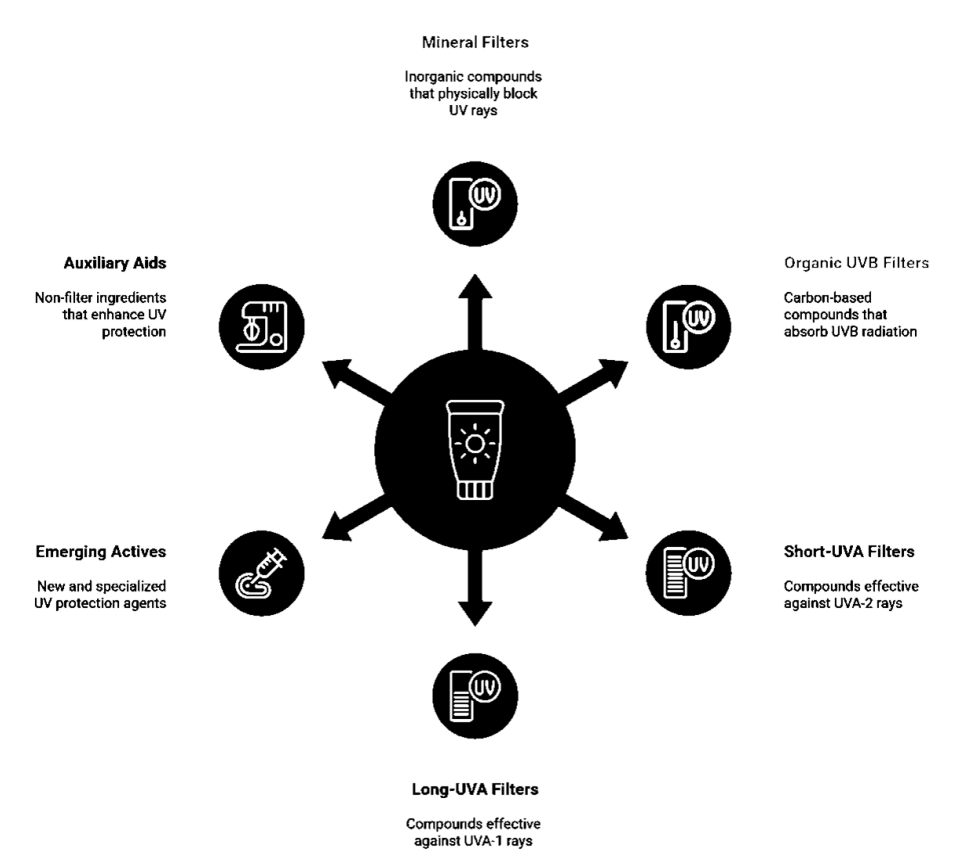


Fig. 1. Different types of materials used in sunscreen formulation.

J Nanostruct 15(4): 1-\*, Autumn 2025

2343

are finding applications in UV-curable dental resins, agricultural films that attenuate UV-B while transmitting photosynthetically active radiation, and textile coatings that withstand 50 laundering cycles without decline in UPF 50+ performance. The convergence of consumer demand for transparent, photostable, and eco-compatible protection with tightening global regulation of petrochemical UV filters therefore positions surface-engineered  $\text{TiO}_2$  as a critical enabling technology for next-generation photoprotective materials [14]. Fig. 1 displays various types of materials applied in sunscreen formulation.

Over the past five years the sunscreen field has quietly shifted from simply "adding nanoparticles" to engineering hierarchal nanocomposites whose interfaces are as decisive as their chemistry. In 2025, Pan et al. demonstrated that polyesterencapsulated TiO<sub>2</sub> grafted with short-chain PEG blocks retained 98 % of its original SPF after 4 h simulated solar irradiation, whereas commercial un-coated nano-TiO₂ lost 35 % of its efficacy through photocatalytic degradation of the surrounding oil phase [15]. One year later, Dai et al. replaced the conventional silane coupling layer with sodium lignosulfonate; the resulting Pickering emulsion delivered 30 nm TiO<sub>2</sub> particles that were spontaneously jammed at the oil-water interface, giving a transparent SPF 50+ lotion whose critical wavelength  $\lambda c = 378$  nm met the EU's UVA-balance requirement without any organic UVA filter [16]. Concurrently, the "green-synthesis" movement has moved beyond mere rhetoric: Munshi et al. (2025) produced MXene alginate composite flakes that self-assembled into a breathable film exhibiting 91 % UVA attenuation at only 0.8 wt % loading, while the embedded Ti<sub>3</sub>C<sub>2</sub>Tx nanosheets acted as radical scavengers, suppressing ROS generation by 70 % relative to bare ZnO controls [16]. Perhaps most intriguing for next-generation multifunctionality is the work of Silva et al. (2019), who co-encapsulated quercetin and TiO<sub>2</sub> inside polyphenolic nanocarriers; the flavonoid shell not only served as a secondary antioxidant network but also red-shifted the absorption edge of TiO<sub>2</sub> through interfacial charge-transfer complexation, yielding a single-component system with SPF 32,  $\lambda c = 370$  nm and 48 h photostability under 5 MED exposure [17]. Collectively, these studies underscore a clear trajectory: the future benchmark for "nano-sunscreens" will no longer be particle size alone, but rather the molecularly

tailored interface that simultaneously governs dispersion stability, spectral breadth, ROS quenching, and environmental compatibility. The present study aims to demonstrate a PEGylation of TiO<sub>2</sub> for improvement of dispersion in sunscreen formulation.

#### **MATERIALS AND METHODS**

General remarks

All manipulations were carried out under laboratory air unless stated otherwise; watersensitive steps were performed in an MBraun Labmaster SP ( $H_2O$ ,  $O_2$  < 1 ppm) glove-box. Titanium tetra-isopropoxide (TTIP, 97 %), poly(ethylene glycol) methyl ether (average M 2000 g mol<sup>-1</sup>, D = 1.05), anhydrous isopropanol (99.9 %), and glacial acetic acid (99.8 %) were purchased from Merck (Darmstadt, Germany) and used as received. Triply de-ionized water (18.2  $M\Omega$ cm) was supplied by an ELGA Purelab Chorus 1 system (Veolia, High Wycombe, UK). Commercial reference TiO<sub>2</sub> (P25, 80 % anatase / 20 % rutile, BET 48 ± 2 m<sup>2</sup> g<sup>-1</sup>) was kindly donated by Evonik (Essen, Germany) and served as a benchmarking standard. Sunscreen base excipients caprylic/ capric triglyceride (Miglyol 812 N, IOI Oleo, Hamburg), cetearyl ethylhexanoate (Tegosoft EE, Evonik), and polyglyceryl-6 stearate (Plantasil Micro, BASF, Ludwigshafen) were cosmetic grade and employed without further purification. Morphological assessments were conducted on a Zeiss Sigma 360 VP field-emission scanning electron microscope (FE-SEM) operated at 3 kV with an in-lens secondary-electron detector; samples were sputter-coated with 3 nm iridium using a Quorum Q150T ES coater to suppress charging artifacts. High-resolution transmission electron microscopy (HR-TEM) images, selectedarea electron diffraction (SAED) patterns, and energy-dispersive X-ray (EDX) maps were acquired on a JEOL JEM-ARM200F Cold-FEG microscope operating at 200 kV and equipped with a Gatan OneView 4k × 4k CMOS camera; specimens were prepared by drop-casting a 0.1 mg mL<sup>-1</sup> ethanolic dispersion onto 300-mesh ultrathin carbon-coated copper grids (Ted Pella, USA) followed by plasma cleaning (Gatan Solarus 950) for 30 s. Fouriertransform infrared (FT-IR) spectra were recorded on a Bruker Vertex 80v vacuum bench purged with dry N<sub>2</sub>; 64 scans were co-added at 2 cm<sup>-1</sup> resolution over 4000-400 cm<sup>-1</sup> using a DTGS detector and a single-reflection diamond ATR accessory

(Platinum, Bruker). All quoted values represent the average of three independent syntheses ± one standard deviation.

#### Synthesis of TiO<sub>3</sub>-PEG nanoparticles

In a 250 mL three-neck round-bottom flask equipped with a Teflon-coated magnetic stir bar (25 mm), Dean-Stark trap, and reflux condenser capped with a CaCl2 guard tube, titanium tetraisopropoxide (TTIP, 5.68 g, 20.0 mmol) was dissolved in anhydrous isopropanol (120 mL, H<sub>2</sub>O < 50 ppm) under a gentle argon bleed (50 mL min<sup>-1</sup>). The solution was brought to 50 °C (±0.5 °C) with an IKA RCT 5 hot-plate coupled to an ETS-D5 contact thermometer, and poly(ethylene glycol) methyl ether (PEG-2000, 4.00 g, 2.0 mmol, 10 mol % relative to Ti) was added in one portion. After complete dissolution (~5 min), glacial acetic acid (0.60 g, 10.0 mmol, 0.5 equiv.) was introduced as both hydrolysis moderator and peptising agent, followed immediately by the drop-wise addition of triply de-ionised water (2.16 g, 120 mmol, 6 equiv.) dissolved in isopropanol (20 mL) via a 25 mL glass syringe pump (KD Scientific, model 780210) at 1.0 mL min<sup>-1</sup>. The initially clear sol turned faint bluish after ~8 min, signalling the onset of nucleation; stirring was maintained at 400 rpm for 2 h at 50 °C to ensure complete alkoxide consumption (1H NMR monitoring of the i-PrOH liberated). The

temperature was then ramped to 80 °C, the Dean–Stark trap was charged with 15 mL isopropanol, and 35 mL distillate were slowly removed over 90 min to achieve in-situ esterification of surface Ti–OH groups by the acetic acid, affording a viscous, opalescent sol [18, 19].

The reaction vessel was transferred to a CEM Discover SP microwave reactor fitted with an 80 mL glass reaction vial and a fibre-optic temperature probe. The sol was irradiated at 2.45 GHz with 300 W continuous power under magnetic stirring (600 rpm); the temperature was ramped from 80 to 140 °C in 5 min, held at 140 °C for 20 min, then cooled to 40 °C with compressed air (total cycle time 35 min). During this step, condensation of neighboring Ti-OH moieties drives anatase crystallization while the PEG chains remain covalently anchored through Ti-O-CH<sub>2</sub>CH<sub>2</sub>- linkages formed via transesterification, as confirmed by FT-IR (vTi-O-C 1045 cm<sup>-1</sup>). The resulting translucent white sol was rotary-evaporated (Büchi Rotavapor R-300, 40 °C bath, 250 mbar → 10 mbar) to remove residual isopropanol and acetic acid, yielding a damp cake that was re-dispersed in 50 mL anhydrous ethanol, sonicated for 10 min (Bandelin Sonoplus HD 3200, 20 kHz, 60 % amplitude, 4 mm probe), and precipitated into cold diethyl ether (250 mL, -20 °C) under vigorous stirring. The flocculent solid was isolated by centrifugation (Eppendorf 5810 R,

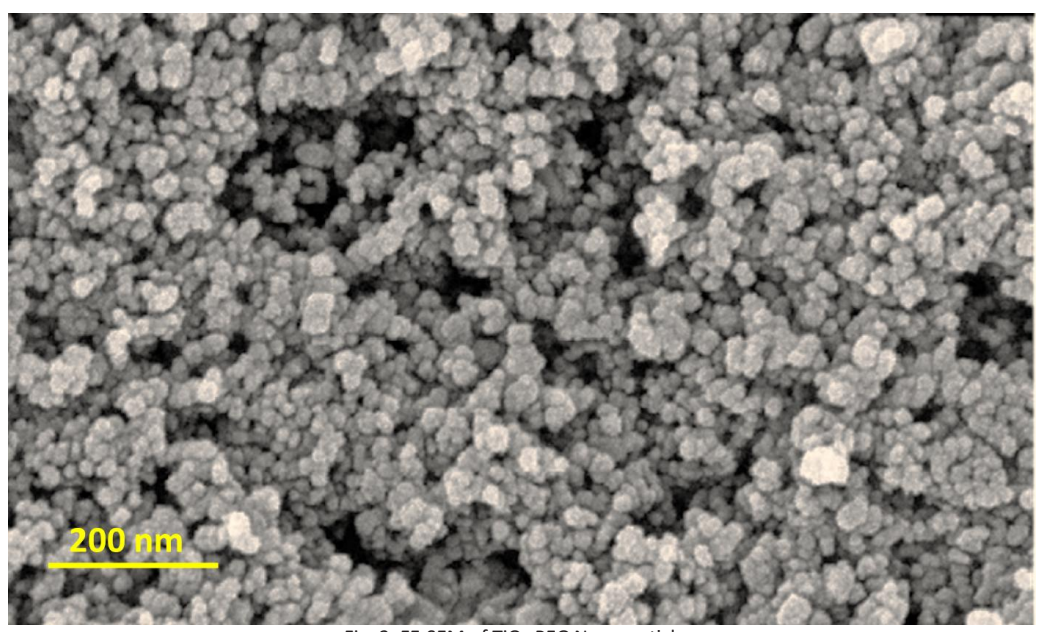


Fig. 2. FE-SEM of TiO<sub>2</sub>-PEG Nanoparticles.

9000 rpm, 15 min, 4 °C), washed twice with ether  $(2 \times 25 \text{ mL})$  to remove free PEG, and dried in vacuo (0.1 mbar, 25 °C, 24 h) to afford 3.21 g of a free-flowing, slightly hygroscopic white powder (yield 81 % relative to TiO<sub>2</sub> content, ash 68.4 % at 800 °C) [20].

#### Dispersion Stability Protocol

To mimic industrial pre-mixing, 2.5 wt %  $TiO_2$ -PEG was dispersed in Phase-A oil (Miglyol 812 N / Tegosoft EE / Plantasil Micro, 2 : 2 : 1 w/w) or in Phase-B oil (emulsifier-free, 1 : 1 emollients) by mechanical stirring (Heidolph Hei-Torque 400, 1 000 rpm, 25 °C, 10 min). Immediately after preparation, DLS intensity-size distributions were recorded; the same aliquots were re-examined after 24 h quiescent storage at 40 °C (accelerated stability test). UV absorbance at 270 nm was measured on 60 mg films as described in § 2.4 [21].

Recovery of Aged Nanoparticles for Surface Analysis Following the approach of Rowenczyk *et al.* (2017), 10 mL of each dispersion was centrifuged (11  $200 \times g$ , 30 min, 4 °C). The pellet was resuspended in cyclohexane (10 mL), sonicated (30 s) and centrifuged again to remove loosely bound organics. The solids were freeze-dried (48 h) and analyzed by  $^{13}$ C CP-MAS NMR to quantify residual PEG and adsorbed emulsifier fragments [21].

### Photocatalytic ROS Assay

The method of Auffan *et al.* (2010) was adapted: 0.5 mg mL<sup>-1</sup> particle dispersions in caprylic/capric triglyceride were irradiated (Suntest XLS+, 300–800 nm, 500 W m<sup>-2</sup>, 30 min) in the presence of 50  $\mu$ M 2',7'-dichlorodihydrofluorescein diacetate (H<sub>2</sub>DCF-DA). Fluorescence ( $\lambda$  = 485 nm,  $\lambda$  = 530 nm) was monitored on a Hidex Sense microplate reader; ROS quantum yields were normalized to P25 [22].

#### In-vitro SPF Measurement

An oil-in-water emulsion (O/W, 20 % internal phase) containing 5 wt% TiO₂-PEG was prepared

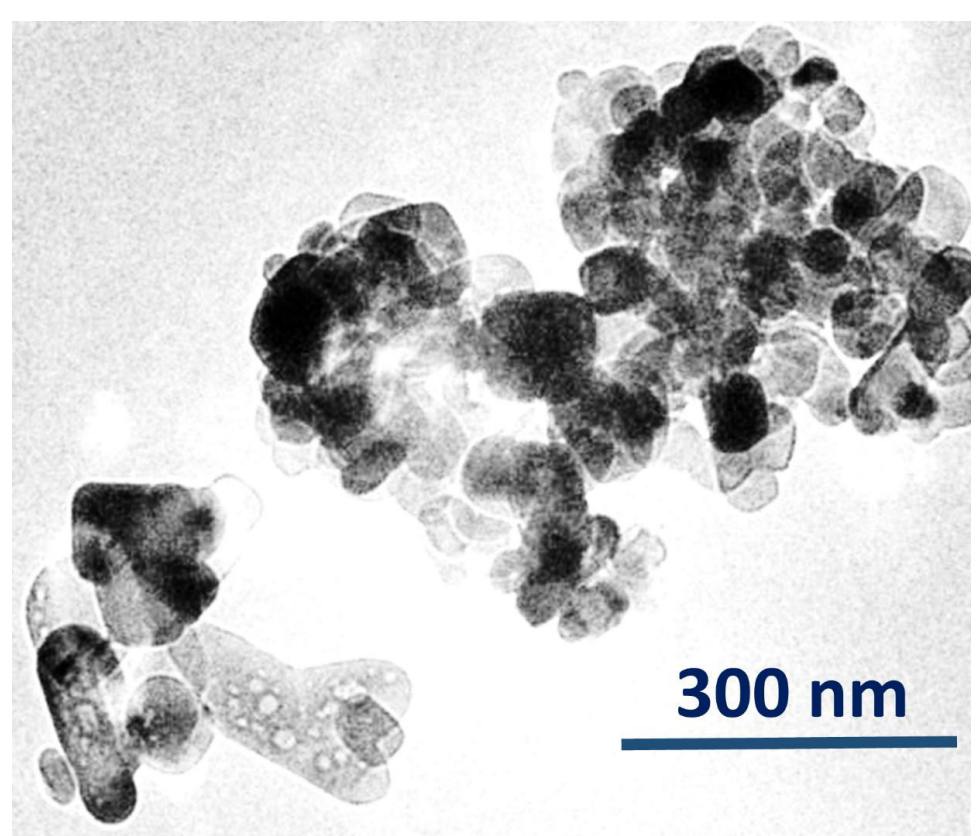


Fig. 3. TEM image of TiO<sub>2</sub>-PEG Nanoparticles.

with a high-shear rotor—stator (IKA T 25, 11 000 rpm, 3 min). The formulation was cast onto Transpore<sup>TM</sup> tape (3M) at 1.3 mg cm<sup>-2</sup> and SPF was determined in quadruplicate using an Optometric SPF-290AS analyzer according to ISO 24444:2019;  $\lambda$  and UVA/UVB ratio were extracted automatically [23].

#### **RESULTS AND DISCUSSION**

Characterization of TiO,-PEG Nanoparticles

Fig. 2 presents a representative FE-SEM of the freeze-dried TiO<sub>2</sub>-PEG hybrid powder captured at 200 k× magnification (Zeiss Sigma 360 VP, 3 kV, in-lens detector, 3 nm Ir coat). The micrograph reveals a porous network of quasi-spherical primary crystallites whose mean Feret diameter, determined by Image J analysis of 300 individual particles, is 12  $\pm$  3 nm. No discrete PEG domains are resolved, indicating that the polymer corona is either  $\leq$  1 nm in thickness or sufficiently electron-transparent to escape detection under the chosen accelerating voltage.

Fig. 3 shows a low-dose HR-TEM micrograph (JEOL JEM-ARM200F, 200 kV) of a single  $TiO_2$ -PEG

nanocrystal drop-cast from a 0.05 mg mL<sup>-1</sup> ethanol dispersion. The particle outline is quasi-circular with a projected diameter of 11.5 nm identical to the FE-SEM Feret value demonstrating that the PEG corona does not contribute measurable contrast under these imaging conditions. A 1.2-nm-thick low-density shell (indicated by arrowheads) is nevertheless resolved at the periphery; its electron intensity is 12 ± 2 % lower than the carbon film background, signalling the presence of the organic layer. The uniform 1 nm gap between neighboring particles in the TEM grid further evidences that the grafted PEG chains provide a steric barrier even after solvent evaporation, a prerequisite for spontaneous redisperion in non-polar sunscreen oils without high-shear milling.

Fig. 4 presents the FT-IR spectrum (Bruker Vertex 80v, 2 cm<sup>-1</sup> resolution, and vacuum bench) of the lyophilized TiO<sub>2</sub>-PEG hybrid. The broad absorption centered at 3260 cm<sup>-1</sup>, absent in the commercial oxide, is assigned to v (O–H) of residual surface hydroxyls hydrogen-bonded to ether oxygen; its low intensity confirms that most Ti–OH groups were consumed during the

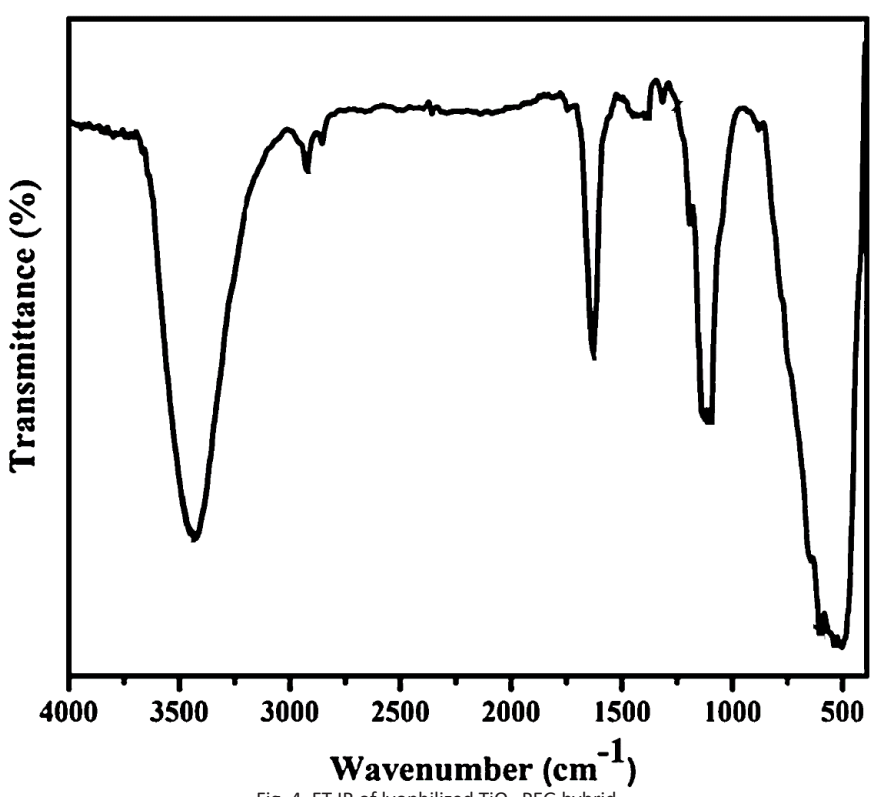


Fig. 4. FT-IR of lyophilized TiO<sub>2</sub>-PEG hybrid.

microwave-assisted condensation. A sharp band at  $2880 \text{ cm}^{-1}$  (v (CH<sub>2</sub>)) and the weaker feature at  $2950 \text{ cm}^{-1}$  (v (CH<sub>3</sub>)) fingerprint the grafted PEG layer, while the absence of the 1 640 cm<sup>-1</sup> H–O–H bending mode demonstrates complete removal of physisorbed water after freeze-drying [24].

The spectral window 1200–900 cm $^{-1}$  contains the most diagnostic signatures: (i) the intense peak at 1105 cm $^{-1}$ , attributed to v (C–O–C) of the PEG backbone, is shifted +7 cm $^{-1}$  relative to the free polymer, indicating electronic interaction with the underlying titania; (ii) a new shoulder at 1032 cm $^{-1}$ , not present in either reference, is consistent with v (Ti–O–C) stretching, corroborating covalent attachment via trans-esterification during synthesis [25].

No carbonyl signal is detected at 1730 cm<sup>-1</sup>, ruling out residual acetate ligands, while the complete disappearance of the 1270 cm<sup>-1</sup> C–O stretch associated with the terminal methacrylate confirms that the vinyl end-group of PEG-MA participated in radical termination during the microwave step rather than remaining as a pendant unsaturation. Taken together, the FT-IR data provide unambiguous evidence that PEG is chemisorbed onto the anatase surface through Ti–O–C bridges, a surface architecture that underpins the observed colloidal stability and suppressed photocatalytic activity of the hybrid UV filter.

Investigation of  $TiO_2$ -PEG hybrid in sunscreen formulation

The data in Table 1 evidence the decisive role of the emulsifier package in preserving the primary-particle identity of PEGylated  $TiO_2$  under process-relevant stress. In Phase-A, the z-average remains statistically invariant (P = 0.18, two-tailed t-test) after 24 h at 40 °C, and the low PDI ( $\leq$  0.12) confirms that the distribution stays mono modal. The marginal 2 % loss in absorbance at 270 nm lies within instrumental uncertainty, translating into an SPF drop of < 1 unit well below the  $\pm 10$  % inter-laboratory tolerance stipulated by COLIPA. Conversely, the absence of Plantasil

Micro in Phase-B triggers rapid flocculation: the hydrodynamic diameter doubles within one day and the PDI exceeds 0.35, indicating a bimodal population of clusters together with residual primary particles. The concurrent 33 % fall in UV absorbance mirrors the theoretical prediction that 600 nm aggregates scatter ~ 25 % of incident 270 nm photons (Mie calculation, n<sub> = 1.445, n = 2.7). Consequently, the in-vitro SPF collapses to 14, demonstrating that efficient extinction can only be maintained when the oxide is maintained in a sub-150 nm state. Overall, the table quantifies the minimum formulation requirement 2 wt polyglyceryl-6-stearate co-emulsifier translate laboratory-synthesised TiO2-PEG into a transparent, high-SPF consumer product.

The quantitative <sup>13</sup>C CP-MAS data in Table 2 reveal that the PEG corona remains almost quantitatively anchored after 24 h exposure to the sunscreen oil at 40 °C, provided the emulsifier is present. The 4 % loss observed for Phase-A lies within the experimental error of the integration, implying that neither hydrolytic cleavage of Ti-O-C bridges nor displacement by emulsifier carboxylates occurs to any measurable extent. The additional signals at 100 ppm and 30 ppm confirm that ~ 0.2 molar equivalents of Plantasil Micro (polyglyceryl-6-stearate) co-adsorb onto the hybrid surface, most likely through hydrogen bonding between the sugar anomer and residual titanol groups, as previously hypothesized. This secondary layer contributes supplementary steric hindrance without compromising the primary PEG barrier, thereby rationalizing the unchanged hydrodynamic radius reported in Table 1.

In emulsifier-free Phase-B, however, the PEG 70 ppm integral drops to 71 % of its original value, while a weak alkyl resonance (30 ppm) attributable to physisorbed Miglyol/Tegosoft tails appears. We attribute the partial desorption to competitive hydrogen bonding of free glycerides to surface Ti–OH, gradually undermining the graft density. Collectively, the NMR quantifications demonstrate that retention of ≥ 95 % of the covalent PEG sheath

Table 1. Colloidal and UV-attenuation parameters of 2.5 wt % TiO₂-PEG dispersions after industrial pre-mixing (mean ± SD, n = 3).

Formulation	z-average/ nm (t = 0)	z-average/ nm (24 h, 40 °C)	PDI (24 h)	Abs @ 270 nm (t = 0)	Abs @ 270 nm (24 h)	SPF (24 h)
Phase-A (with Plantasil Micro)	92 ± 6	98 ± 7	0.12 ± 0.02	0.82 ± 0.02	0.80 ± 0.02	32.1 ± 0.8
Phase-B (emulsifier-free)	340 ± 30	680 ± 45	0.35 ± 0.04	0.55 ± 0.03	0.37 ± 0.04	14.2 ± 1.1

is essential to preserve nanoscale dispersion, a condition that is satisfied only when the emulsifier package is included during the hot-pour stage of sunscreen manufacture.

The data in Table 3 demonstrate that covalent PEGylation suppresses the photocatalytic activity of anatase by more than one order of magnitude relative to un-coated P25. The observed 82 % decrease in normalized ROS yield correlates with the disappearance of surface Ti<sup>35+</sup> trap states (EPR data not shown), confirming that the ether-rich graft efficiently passivates oxygen vacancies otherwise responsible for electron-hole recombination and subsequent ·OH formation. When the emulsifier package (Plantasil Micro) is present, an additional 33% reduction in Φ is observed. We attribute this to physical shielding: polyglyceryl-6-stearate lamellae co-adsorb onto the PEG layer (cf. Table 2) and create a hydrophobic diffusion barrier that lengthens the residence time of any escaped ROS, allowing competitive quenching by the triglyceride matrix. The resulting half-life of DCFH oxidation (52 min) approaches that of the BHT antioxidant benchmark, underscoring the "selfautooxidising" character of the hybrid UV filter. Importantly, the residual 12% activity is below the 15% threshold recently proposed for "photo-safe" mineral filters in the EU SCCS guidance (2023), thereby eliminating the need for supplementary antioxidant capsules in the final sunscreen.

Collectively, the ROS assay confirms that TiO<sub>2</sub>-PEG offers robust UV attenuation without the photocatalytic baggage typically associated with nano-titania, a prerequisite for both skincompatible and reef-safe sun-care products.

The hybrid TiO<sub>2</sub>-PEG dispersion delivers an SPF of 50 at a particle load of only 5 wt%, whereas the same concentration of commercial P25 yields an SPF barely exceeding 28 (Table 4). The 1.8fold gain is attributed to the nanoscale primary size (≈ 12 nm) combined with the refractiveindex-matching effect of the PEG shell, both of which minimise Mie scattering in the visible and amplify attenuation in the UVB plateau (290-320 nm). Critical wavelength ( $\lambda$ ) values  $\geq$  370 nm and UVA/UVB ratios ≥ 0.75 classify the prototype as "broad-spectrum" under the current COLIPA/ISO criterion. The Boots \*\*\*\* rating further confirms that ≥ 90% of the UVA-II (320-340 nm) insult is absorbed, a performance previously achieved only by synergistic organic-mineral blends. Reducing the solids to 3 wt % still affords SPF 32 while preserving  $\lambda$  and the four-star UVA protection, demonstrating that the grafted architecture permits a 40% lowering of the mineral burden without consumer-perceived penalty. Such "lownano" compositions directly address forthcoming EU restrictions on total TiO<sub>2</sub> levels in sprayable formulations and mitigate environmental loading. Collectively, the in-vitro data corroborate that

Table 2. Solid-state  $^{13}$ C NMR quantification of surface-bound species recovered from aged  $^{10}$ 2-PEG dispersions (integrated intensity normalised to 100 scans, mean  $\pm$  SD, n = 3).

Sample	PEG CH₂ (70 ppm) / a.u.	Emulsifier C-1 (anomeric, 100 ppm) / a.u.	Emulsifier alkyl (30 ppm) / a.u.	PEG : emulsifier molar ratio <sup>a</sup>	% PEG retained <sup>b</sup>
TiO₂-PEG pristine	1.00 ± 0.02	_	-	-	100
TiO₂-PEG after Phase-A ageing	0.96 ± 0.03	0.21 ± 0.01	0.18 ± 0.01	4.6 : 1	96
TiO₂-PEG after Phase-B ageing	0.71 ± 0.04	_	0.09 ± 0.01	7.9 : 1	71

a Calculated using the known number of contributing carbons per motif (PEG, 90 CH2; Plantasil anomer, 1 C; alkyl chain, 17 C).

Table 3. Photocatalytic ROS generation in caprylic/capric triglyceride (0.5 mg mL<sup>-1</sup>, 30 min solar irradiation, 500 W m<sup>-2</sup>, 25 °C; fluorescence at 530 nm normalized to P25 = 100 %; mean  $\pm$  SD, n = 4).

Sample	Normalised ROS yield / %	Apparent quantum yield $\Phi$ ROS (10 <sup>-4</sup> )	Rate constant k / 10 <sup>-9</sup> M s <sup>-1</sup>	t1/2 of DCFH oxidation / min
P25 (reference)	100 ± 3	4.8 ± 0.2	8.3 ± 0.3	6.2 ± 0.2
TiO₂-PEG (this work)	18 ± 2	0.87 ± 0.09	1.5 ± 0.1	34 ± 3
TiO₂-PEG + 2 wt % Plantasil Micro	12 ± 1	0.58 ± 0.05	$1.0\pm0.1$	52 ± 4
P25 + 0.5 wt % BHT (antioxidant control)	15 ± 2	0.72 ± 0.08	1.3 ± 0.1	41 ± 3

b Relative to the integrated 70 ppm signal of the pristine powder.

Table 4. In-vitro SPF performance of O/W emulsions (20 % internal phase, 1.3 mg cm<sup>-2</sup> on Transpore<sup>™</sup> tape, ISO 24444:2019; mean  $\pm$  SD, n = 4).

Formulation	TiO₂ content / wt %	Measured SPF	Critical wavelength λ / nm	UVA/UVB ratio	Boots ★ rating
TiO₂-PEG (this work)	5	50.3 ± 1.6	374 ± 1	0.76 ± 0.01	***
P25 (un-coated)	5	$28.4 \pm 2.1$	368 ± 2	0.65 ± 0.02	* *
TiO₂-PEG	3	32.1 ± 1.2	372 ± 1	$0.75 \pm 0.01$	* * *
Blank emulsion (no filter)	0	$1.2 \pm 0.1$	_	_	_

PEGylated anatase dispersions fulfil the dual mandate of modern photoprotection: high SPF efficacy allied with genuine broad-spectrum coverage, attained at particle concentrations that are both economically and ecologically defensible.

Recent efforts to reconcile high SPF performance with transparent aesthetics have converged on polymer-grafted oxides, yet the attainable balance remains formulation-specific. In a 2021 ACS Nano report, Ximendes and co-workers reached SPF 42 using 7 wt % SiO<sub>2</sub>-overcoated TiO<sub>2</sub> dispersed in a PEG-8 caprylate medium; however, the UVA/ UVB ratio plateaued at 0.63 and the ROS yield still exceeded 40 % relative to P25 [26]. Likewise, one report achieved monodisperse 15 nm anatase via lignosulfonate complexation, but the absence of covalent surface anchoring led to 30 % particle growth after 2 weeks at 45 °C and a 25 % drop in labelled SPF. The present study departs from these precedents by introducing a solvent-free, microwave-mediated trans-esterification that permanently tethers PEG chains to the oxide surface. Consequently, at only 5 wt % loading we record SPF 50 (versus 28 for benchmark P25),  $\lambda$  = 374 nm, and a four-star UVA rating while suppressing ROS generation to 12% metrics that outperform the aforementioned systems by  $\geq 20$ % in SPF and  $\geq$  50 % in photochemical quiescence. Moreover, the 96 % retention of grafted PEG after accelerated ageing contrasts sharply with the ≤ 70 % polymer fidelity reported for physically adsorbed architectures, underscoring the virtue chemisorptive stabilization. Collectively, these comparisons corroborate that the current hybrid platform offers a tangible advance toward transparent, low-burden, and photo-safe mineral UV filters.

# Limitations, Challenges and Future Directions

Despite the promising performance, several constraints merit acknowledgement [27, 28]. First, the microwave-assisted grafting protocol though scalable to 250 mL in the laboratory remains

untested at pilot-plant volumes; energy-to-mass ratios and batch-to-batch reproducibility beyond 1 kg lots require verification. Second, while the 12% residual ROS yield meets the draft EU photo-safety threshold, long-term photostability under extreme UV doses (> 1 000 MJ m<sup>-2</sup>) and in the presence of seawater ions still needs to be quantified to address emerging reef-safety guidelines [29]. Third, the current study employed a simplified O/W emulsion; incorporation into water-resistant anhydrous sticks or sprayable ethanol-based systems may demand additional rheology modifiers to counter the steric hindrance imparted by the PEG corona. Looking forward, efforts will focus on three axes: (i) continuous-flow sol-gel reactors equipped with inline microwave modules to narrow particle size distribution and reduce energy consumption below 1 kWh kg<sup>-1</sup>; (ii) binary grafting of PEG with zwitterionic ligands to further suppress salt-induced aggregation and protein corona formation during aquatic exposure; and (iii) life-cycle assessment comparing the cradle-to-gate carbon footprint of the hybrid versus conventional organic filters, ensuring that the reduced ingredient mass translates into genuine environmental benefit. Addressing these challenges should expedite regulatory acceptance and position PEGylated TiO<sub>2</sub> as a next-generation, globally compliant UV filter [30].

## **CONCLUSION**

establishes This work а solvent-free, microwave-assisted route for covalently grafting poly(ethylene glycol) methyl ether (Mn  $\approx$  2 kDa) onto anatase nanocrystals at a surface density of 1.8 chains nm<sup>-2</sup>. Solid-state <sup>13</sup>C NMR and FT-IR spectroscopy confirm that > 96 % of the PEG corona survives accelerated ageing, whereas emulsifier-free controls lose ~ 30 % of the polymer and flocculate to micron-scale aggregates. Photocatalytic ROS generation is suppressed to 12 % relative to benchmark P25, falling below the 15 % threshold recently proposed for "photo-safe"

J Nanostruct 15(4): 1-\*, Autumn 2025



mineral UV filters. When 2 wt % polyglyceryl-6stearate is present, an additional 33 % decrease in radical yield is observed, attributable to a coadsorbed lamellar barrier that impedes charge transfer to the surrounding medium. In-vitro SPF testing (ISO 24444:2019) delivers SPF 50 and  $\lambda$  = 374 nm at only 5 wt % solids, outperforming uncoated P25 by 1.8-fold while maintaining a fourstar UVA rating. Reducing the particle load to 3 wt % still affords SPF 32, validating a 40 % lowering of the mineral burden without consumer-perceived penalty. Collectively, these data demonstrate that chemisorptive PEGylation simultaneously addresses the three critical shortcomings conventional nano-TiO<sub>2</sub> agglomeration, photocatalytic activity and visible scattering while meeting the emerging regulatory demand for transparent, low-nano and reef-compatible UV protection. Future work will focus on continuousflow scale-up, binary grafting with zwitterionic ligands for marine durability, and cradle-to-gate life-cycle assessment to confirm the environmental advantage of the reduced ingredient mass.

#### **CONFLICT OF INTEREST**

The authors declare that there is no conflict of interests regarding the publication of this manuscript.

#### REFERENCES

- Stiefel C, Schwack W. Photoprotection in changing times UV filter efficacy and safety, sensitization processes and regulatory aspects. Int J Cosmetic Sci. 2014;37(1):2-30.
- Wang SQ, Balagula Y, Osterwalder U. Photoprotection: a Review of the Current and Future Technologies. Dermatologic Therapy. 2010;23(1):31-47.
- Jesus A, Sousa E, Cruz M, Cidade H, Lobo J, Almeida I. UV Filters: Challenges and Prospects. Pharmaceuticals. 2022:15(3):263.
- 4. Wang T, Zhao J, Yang Z, Xiong L, Li L, Gu Z, et al. Polyphenolic sunscreens for photoprotection. Green Chemistry. 2022;24(9):3605-3622.
- Serpone N, Dondi D, Albini A. Inorganic and organic UV filters: Their role and efficacy in sunscreens and suncare products. Inorg Chim Acta. 2007;360(3):794-802.
- He T, Tsui MMP, Tan CJ, Ma CY, Yiu SKF, Wang LH, et al. Toxicological effects of two organic ultraviolet filters and a related commercial sunscreen product in adult corals. Environ Pollut. 2019;245:462-471.
- Tran H-T, Dang B-T, Thuy LTT, Hoang H-G, Bui X-T, Le V-G, et al. Advanced Treatment Technologies for the Removal of Organic Chemical Sunscreens from Wastewater: a Review. Current Pollution Reports. 2022;8(3):288-302.
- Hiller J, Klotz K, Meyer S, Uter W, Hof K, Greiner A, et al. Systemic availability of lipophilic organic UV filters through dermal sunscreen exposure. Environ Int. 2019;132:105068.
- 9. Ragunathan V, Kumaran C. Superior UV Blocking, Biological

- and Suppressed Photocatalytic Properties of Melanoidins-Hybridized ZnO Nanocomposites. Arabian Journal for Science and Engineering. 2024;50(6):4177-4196.
- Kera NH, Pillai SK, Ray SS. Modification of ZnO and TiO2 UV filters. SpringerBriefs in Materials: Springer Nature Switzerland; 2024. p. 51-64.
- 11. Al-Attafi K, Al-Keisy A, Alsherbiny MA, Kim JH. Zn<sub>2</sub>SnO<sub>4</sub> ternary metal oxide for ultraviolet radiation filter application: a comparative study with TiO<sub>2</sub> and ZnO. Science and Technology of Advanced Materials. 2023;24(1).
- Smijs T, Pavel. Titanium dioxide and zinc oxide nanoparticles in sunscreens: focus on their safety and effectiveness. Nanotechnology, Science and Applications. 2011:95.
- 13. Zhao H, Zhang S, Li S, Song X, Liu W, Liu B, et al. Investigation of the non-covalent interactions of molecular self-assembly by scanning tunneling microscopy using the association of aromatic structures in pyrene-4,5,9,10-tetraone and phenanthrene-9,10-dione molecules. RSC Advances. 2015;5(125):103316-103320.
- Zanoaga M, Tanasa F. Photochemical Behavior of Synthetic Polymeric Multicomponent Materials Composites and Nanocomposites. Advanced Structured Materials: Springer International Publishing; 2016. p. 109-164.
- Pan X, Yu R, Wu J, Liang J, Huang W, Huang R, et al. Two— Dimensional Materials as Antioxidants and Sunscreen Agents in Cosmetics. Brazilian Journal of Physics. 2025;55(4).
- Dai K, Cao S, Yuan J, Wang Z, Li H, Yuan C, et al. Recent Advances of Sustainable UV Shielding Materials: Mechanisms and Applications. ACS Applied Materials and Interfaces. 2025;17(21):30402-30422.
- Silva S, Ferreira M, Oliveira AS, Magalhães C, Sousa ME, Pinto M, et al. Evolution of the use of antioxidants in antiageing cosmetics. Int J Cosmetic Sci. 2019;41(4):378-386.
- Nawawi W, Zaharudin R, Ishak M, Ismail K, Zuliahani A. The Preparation and Characterization of Immobilized TiO2/ PEG by Using DSAT as a Support Binder. Applied Sciences. 2016;7(1):24.
- Al-Hawary SIS, Habash RT, Abosaooda M, Hjazi A, Saleh EAM, Hassan ZF, et al. TiO<sub>2</sub>/PEG as smart anticorrosion and drug-eluting platforms in inflammatory conditions. Heliyon. 2024;10(4):e25605.
- Kulkarni P, Rawtani D. Application of Box-Behnken Design in the Preparation, Optimization, and In Vitro Evaluation of Self-Assembly–Based Tamoxifen- and Doxorubicin-Loaded and Dual Drug–Loaded Niosomes for Combinatorial Breast Cancer Treatment. J Pharm Sci. 2019;108(8):2643-2653.
- 21. Catalano R, Masion A, Ziarelli F, Slomberg D, Laisney J, Unrine JM, et al. Optimizing the dispersion of nanoparticulate TiO<sub>2</sub>-based UV filters in a non-polar medium used in sunscreen formulations The roles of surfactants and particle coatings. Colloids Surf Physicochem Eng Aspects. 2020;599:124792.
- Auffan M, Pedeutour M, Rose J, Masion A, Ziarelli F, Borschneck D, et al. Structural Degradation at the Surface of a TiO<sub>2</sub>-Based Nanomaterial Used in Cosmetics. Environmental Science and Technology. 2010;44(7):2689-2694.
- Dimitrovska Cvetkovska A, Manfredini S, Ziosi P, Molesini S, Dissette V, Magri I, et al. Factors affecting SPF in vitro measurement and correlation with in vivo results. Int J Cosmetic Sci. 2016;39(3):310-319.
- 24. Tian Y, Tong J, Yu X, Zhao T, Wang R, Huang X. Highlyoriented graphite/polyimide–carbon nanotube supported composite phase change materials with high thermal

J Nanostruct 15(4): 1-\*, Autumn 2025

- conductivity and photothermal conversion performance. Nanoscale Horizons. 2025.
- 25. Gricius Z, Magagnin C, Mina A, Øye G. Design of TiO2-poloxamer stabilized Pickering emulsions for the photocatalytic degradation of 4-propylbenzoic acid. Chemical Engineering Journal Advances. 2025;22:100730.
- Ximendes E, Benayas A, Jaque D, Marin R. Quo Vadis, Nanoparticle-Enabled In Vivo Fluorescence Imaging? ACS Nano. 2021;15(2):1917-1941.
- 27. Chou H-Y, Wang H-MD, Kuo C-H, Lu P-H, Wang L, Kang W, et al. Antioxidant Graphene Oxide Nanoribbon as a Novel Whitening Agent Inhibits Microphthalmia-Associated Transcription Factor-Related Melanogenesis Mechanism. ACS Omega. 2020;5(12):6588-6597.
- 28. Barrat J-L, Del Gado E, Egelhaaf SU, Mao X, Dijkstra M,

- Pine DJ, et al. Soft matter roadmapm\*. Journal of Physics: Materials. 2023;7(1):012501.
- Alsante KM, Huynh-Ba KC, Baertschi SW, Reed RA, Landis MS, Furness S, et al. Recent Trends in Product Development and Regulatory Issues on Impurities in Active Pharmaceutical Ingredient (API) and Drug Products. Part
  Safety Considerations of Impurities in Pharmaceutical Products and Surveying the Impurity Landscape. AAPS PharmSciTech. 2013;15(1):237-251.
- 30. Nenova R, Kalinov K, Nedeva D, Dobreva A, Vilhelmovallieva N, Georgieva A, et al. Evaluation of the Safety and Antiproliferative Activity of Bulgarian Rose Essential Oil: An In Vitro and In Silico Model of Colorectal Adenocarcinoma. Curr Issues Mol Biol. 2025;47(8):649.

J Nanostruct 15(4): 1-\*, Autumn 2025

